Direct observations of Ca ordering in $Ca_{0.33}CoO_2$ thin films with different superstructures

Rong Huang,[1,a)] Teruyasu Mizoguchi,[2] Kenji Sugiura,[3] Hiromichi Ohta,[3] Kunihito Koumoto,[3] Tsukasa Hirayama,[1] and Yuichi Ikuhara[1,2]
[1]*Nanostructures Research Laboratory, Japan Fine Ceramics Center, Atsuta, Nagoya 456-8587, Japan*
[2]*Institute of Engineering Innovation, The University of Tokyo, Bunkyo, Tokyo 113-8656, Japan*
[3]*Graduate School of Engineering, Nagoya University, Chikusa, Nagoya 464-8603, Japan*

(Received 2 September 2008; accepted 19 October 2008; published online 5 November 2008)

Ca-ion superstructures such as $\sqrt{3}a\times\sqrt{3}a$ (hexagonal) and $2a\times\sqrt{3}a$ (orthorhombic) in layered $Ca_{0.33}CoO_2$ crystalline film, which were prepared by the reactive solid-phase epitaxy and the subsequent ion-exchange treatment, were directly distinguished by using spherical-aberration-corrected high-angle annular dark-field scanning transmission electron microscopy (HAADF-STEM). The fluctuation of Ca intensities in the HAADF-STEM image indicates the existence of many Ca vacancies in the $2a\times\sqrt{3}a$ orthorhombic superstructure, which is consistent with the partial occupation of Ca ($x=0.33$) in the cation sites of $x=0.5$. © *2008 American Institute of Physics*. [DOI: 10.1063/1.3021369]

Layered cobalt oxide, M_xCoO_2 (M=Li, Na, Ca, Sr), has attracted increasing research interest due to their high potentials for thermoelectric devices, battery cathodes, superconductor, and other electric and magnetic applications.[1–10] These layered cobalt oxides commonly consist of alternately stacked sheets of alkaline/alkaline earth ions and CoO_2^- layers along the c-axis direction, as shown in Fig. 1. The alkaline/alkaline earth ion content and crystal structures can vary over a wide range by ionic intercalation and exchanges, and the physical properties are a function of the concentration and ordering of the cations.[11–14] Therefore, many studies have focused on the intercalated alkaline/alkaline earth ions, vacancy ordering, and physical properties of the layered cobalt oxide material.[15–18]

Yang *et al.*[19] performed high resolution transmission electron microscopy studies of Ca_xCoO_2 and identified two well-defined ordered structures, $\sqrt{3}a\times\sqrt{3}a$ hexagonal superstructure and $2a\times\sqrt{3}a$ orthorhombic superstructure, respectively, and that the ordered superstructure depended on the concentration of Ca. More recently, Sugiura *et al.*[20] fabricated high quality Ca_xCoO_2 thin films with the $\sqrt{3}a\times\sqrt{3}a$ hexagonal and $2a\times\sqrt{3}a$ orthorhombic superstructures in spite of the fact that both had the same Ca concentration ($x=0.33$). Thus, an atomic scale understanding of the ordered structure in the layered cobalt oxides is still controversial.

In this study, direct observation of the ordered structure of the intercalated cations and/or vacancies in $Ca_{0.33}CoO_2$ was attempted by using high-angle annular dark-field scanning transmission electron microscopy (HAADF-STEM) techniques. HAADF-STEM has the advantage that the image contrast is roughly proportional to the atomic number (Z).[21,22] It is suitable for direct observation of the cation ordering in these layered cobalt oxides and can provide invaluable information to understand the relationship between cation ordering and physical properties at the atomic scale. In the present study, this powerful technique is used to observe the ordered structure of Ca and vacancies in $Ca_{0.33}CoO_2$ epitaxial films. Furthermore, effects of the vacancies on the local atomic structures are discussed.

The $Ca_{0.33}CoO_2$ epitaxial films were fabricated by the topotactic ion-exchange treatment using a $Na_{0.7}CoO_2$ epitaxial film as a precursor, which was grown on the c (0001) plane of α-Al_2O_3 by the reactive solid-phase epitaxy method. Details of film growth are described elsewhere.[20,23,24] Cross-sectional TEM specimens were characterized in a JEOL JEM-3000F microscope equipped with a field emission gun operating at 300 kV for selected-area electron diffraction (SAED) analysis and a JEOL JEM-2100F equipped with a spherical aberration corrector (CEOS Gmbh) and a parallel electron energy-loss spectroscopy (EELS) system (Gatan Enfina) for HAADF-STEM observations.

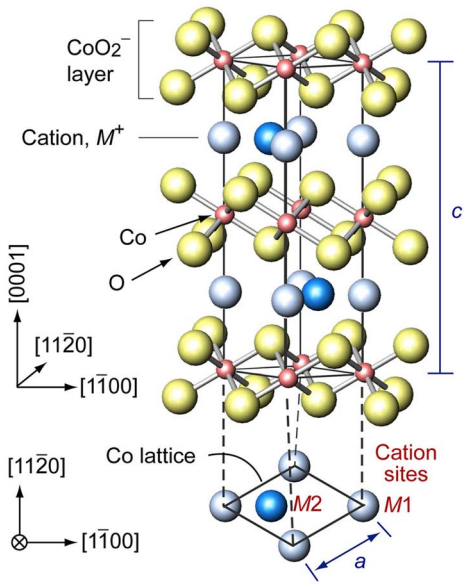

FIG. 1. (Color online) Schematic crystal structure of a layered cobalt oxide M_xCoO_2 (M=Na or Ca). There are two sites for the cations, denoted as $M1$ and $M2$. The lattice parameters of the $Ca_{0.33}CoO_2$ thin film are $a=0.282$ nm and $c=1.086$ nm, respectively.

a)Electronic mail: huang@jfcc.or.jp.

 © 2008 American Institute of Physics

Downloaded 28 Jul 2009 to 133.6.32.19. Redistribution subject to AIP license or copyright; see http://apl.aip.org/apl/copyright.jsp

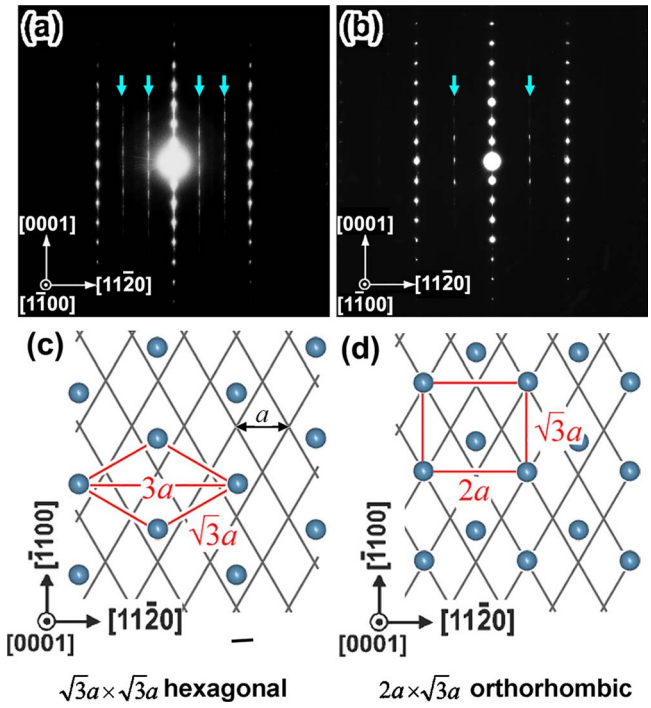

FIG. 2. (Color online) SAED patterns taken along the [1$\bar{1}$00] zone axes. (a) The $\sqrt{3}a \times \sqrt{3}a$ superstructure and (b) the $2a \times \sqrt{3}a$ superstructure. Arrows indicate the superlattice reflections from Ca ordering. Schematics of the Ca ordering in the intercalation plane: (c) the $\sqrt{3}a \times \sqrt{3}a$ hexagonal superstructure and (d) the $2a \times \sqrt{3}a$ orthorhombic superstructure.

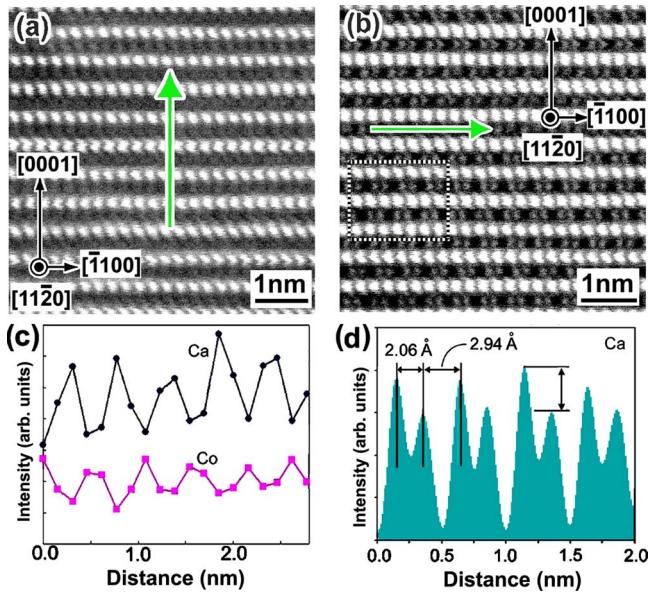

FIG. 3. (Color online) HAADF-STEM images of (a) the $\sqrt{3}a \times \sqrt{3}a$ hexagonal superstructure and (b) the $2a \times \sqrt{3}a$ orthorhombic superstructure along the [11$\bar{2}$0] zone axes. (c) EELS line scan along the arrow line in (a). (d) Intensity profile of the arrow line in (b).

In the Ca_xCoO_2 system, two kinds of well-defined superstructure phases have been reported to exist at around $x=1/3$ and 1/2, corresponding to the $\sqrt{3}a \times \sqrt{3}a$ hexagonal superstructure and the $2a \times \sqrt{3}a$ orthorhombic superstructures, respectively.[19] In-plane x-ray diffraction (XRD) analyses revealed that the as-prepared $Ca_{0.33}CoO_2$ film formed the $\sqrt{3}a \times \sqrt{3}a$ hexagonal superstructure as expected. However, after annealing at 400 °C for 1 h in air, the structure changes to the $2a \times \sqrt{3}a$ orthorhombic superstructure although having the same Ca concentration of $x=0.33$ [measured by x-ray fluorescence (XRF)].[20] Figure 2(a) shows a SAED pattern of the as-prepared $Ca_{0.33}CoO_2$ film when the electron beam is parallel to the [1$\bar{1}$00] zone axes. The superlattice reflections (marked by arrows) appearing at 1/3 and 2/3 of [11$\bar{2}$0], which are due to the Ca ordering, clearly indicate the presence of the $\sqrt{3}a \times \sqrt{3}a$ superstructure. On the other hand, Fig. 2(b) shows a SAED pattern obtained from the annealed $Ca_{0.33}CoO_2$ film along the [1$\bar{1}$00] zone axis. The superlattice reflections (marked by arrows) show the presence of the $2a \times \sqrt{3}a$ superstructure of Ca ions, which is consistent with the in-plane XRD results.[20] The Ca orderings in the intercalation plane of both superstructures are illustrated in Figs. 2(c) and 2(d). It can be clearly seen that these two superstructures are discriminated if Ca ions are observed with the atomic level resolution along the [11$\bar{2}$0] and [1$\bar{1}$00] zone axes. Especially, when these superstructures are observed from the [11$\bar{2}$0] direction, the pair contrast of Ca ions and clear Co columns can be imaged at the same time in the HAADF-STEM image. Accordingly, the [11$\bar{2}$0] direction is chosen here to perform the HAADF-STEM observation.

Figure 3(a) shows a typical HAADF-STEM image of the $\sqrt{3}a \times \sqrt{3}a$ hexagonal superstructure. It is clearly seen that the thin film is composed of alternative stacking of bright layer and in-between dark layer. Considering the contrast due to the atomic number (Z), this difference is too large because Z of Co (27) is close to that of Ca (20). In order to identify the layer composition, EELS line scan analysis with atomic level resolution [Fig. 3(c)] was performed along the arrow line in Fig. 3(a). The line in pink (or gray) and the line in black represent the integrated intensities of the Co $L_{2,3}$ edge and Ca $L_{2,3}$ edge, respectively. The peak positions of Co and Ca, which correspond to bright layers and dark layers in the HAADF-STEM image, appear alternatively and match very well. This dark contrast of the Ca layer is believed to originate from the lower occupancy and more dechanneling of the Ca layer. As discussed later, this is strongly related to the ordered structure of the Ca and vacancy.

The HAADF-STEM image shown in Fig. 3(b) exhibits the arrangement of Ca ions in the $2a \times \sqrt{3}a$ orthorhombic superstructure, which is very different from that in the $\sqrt{3}a \times \sqrt{3}a$ hexagonal superstructure when observed along the [11$\bar{2}$0] zone axes. It clearly shows that the Ca ions are shifted to form the pair contrast. The difference in the location of the Ca site can be used to distinguish the $2a \times \sqrt{3}a$ orthorhombic superstructure from the $\sqrt{3}a \times \sqrt{3}a$ hexagonal superstructure. In order to get more detailed information about the local structure of the Ca layer, we made an intensity profile along the arrow line in Fig. 3(b). From the intensity of each Ca column, the Ca pairs can be also identified, as shown in Fig. 3(d). On the other hand, the intensities of Ca columns are not uniform but fluctuate with relatively large amplitudes, which indicates that there are different numbers of Ca^{2+} ions along the electron beam direction in each Ca column. It might be that some Ca vacancies formed in the $Ca_{0.33}CoO_2$ thin film. In fact, the $2a \times \sqrt{3}a$ orthorhombic superstructure has cation sites of $x=0.5$.[19] However, the concentration of Ca in the present sample is $x=0.33$, which can

Downloaded 28 Jul 2009 to 133.6.32.19. Redistribution subject to AIP license or copyright; see http://apl.aip.org/apl/copyright.jsp

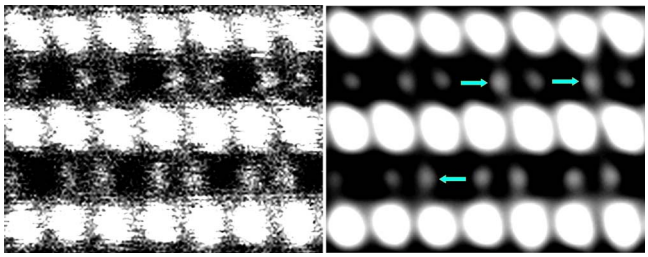

FIG. 4. (Color online) Magnified HAADF-STEM image and corresponding FFT filtered image of the $2a \times \sqrt{3}a$ orthorhombic superstructure along the $[11\bar{2}0]$ zone axes from the dashed rectangle in Fig. 3(b). Arrows are brighter Ca2 sites.

only partly occupy the Ca sites in the $2a \times \sqrt{3}a$ orthorhombic superstructure, leaving many Ca vacancies in the structure. The percentage of Ca vacancies is estimated to be ~34% from the Ca concentration in the film. The short and long Ca–Ca distances measured from the HAADF-STEM image are 2.06 ± 0.09 and 2.94 ± 0.10 Å, respectively. The ratio between the long and short Ca–Ca distances is 1.43 ± 0.09, which is smaller than the ratio of 2 in the ideal structure.[12] It indicates that Ca atoms must have shifted away from each other due to Coulomb interaction among Ca^{2+} ions caused by the Ca vacancies. Thus the variation in the Ca–Ca distance would be related to the distribution of Ca vacancies in this structure. This represents additional evidence for the existence of Ca vacancy.

Similar to Na_xCoO_2,[13] there are two distinct cation sites within a given plane in this layered cobalt oxide; these are denoted as Ca1 and Ca2. The Ca1 site, which lies in between two adjacent cobalt ions (Fig. 1), requires an extra energy cost for occupation relative to Ca2 due to the relatively large electrostatic repulsion between the adjacent Ca^{2+} and Co^{3+}/Co^{4+} ions.[13] This means that the Ca2 site is more stable than the Ca1 site. When Ca vacancies form in the $2a \times \sqrt{3}a$ orthorhombic superstructure, the Ca1 site is preferable. It is consistent with the brighter contrast of Ca2 sites in the HAADF-STEM image shown in Fig. 4 [raw data with fast Fourier transform (FFT) filtered image], taken from the dashed rectangle in Fig. 3(b). Thus, the HAADF-STEM observations have confirmed the existence of Ca vacancies in the $2a \times \sqrt{3}a$ orthorhombic superstructure from various aspects. This is a very important information for understanding the physical properties of these layered cobalt oxides.

In summary, Ca orderings in the $Ca_{0.33}CoO_2$ thin films with the $\sqrt{3}a \times \sqrt{3}a$ hexagonal superstructure and the $2a \times \sqrt{3}a$ orthorhombic superstructure along the $[11\bar{2}0]$ zone axes have been observed by using HAADF-STEM. The $2a \times \sqrt{3}a$ orthorhombic superstructure can be easily differentiated from the $\sqrt{3}a \times \sqrt{3}a$ superstructure from the contrast of Ca pairs in the HAADF-STEM image. The fluctuation of Ca intensities in the HAADF-STEM image reveals the existence of many Ca vacancies in the $2a \times \sqrt{3}a$ orthorhombic superstructure. This study clearly demonstrated that the HAADF-STEM and EELS approaches can identify those important superstructures in the layered cobalt oxides. We are confident that the atomic scale understanding of the ordered structure as presented in this study can pave the way for further development and application of these layered cobalt oxides.

The authors would like to thank Dr. Kenji Nomura and Professor Hideo Hosono for XRF measurements. A part of this study was supported by the Grant-in-Aid for Scientific Research on Priority Areas "Nano Materials Science for Atomic-scale Modification 474" from the Japanese Ministry of Education, Culture, Sports and Technology.

[1] I. Terasaki, Y. Sasago, and K. Uchinokura, Phys. Rev. B **56**, R12685 (1997).
[2] T. Motohashi, E. Naujalis, R. Ueda, K. Isawa, M. Karppinen, and H. Yamauchi, Appl. Phys. Lett. **79**, 1480 (2001).
[3] Y. Wang, N. S. Rogado, R. J. Cava, and N. P. Ong, Nature (London) **423**, 425 (2003).
[4] M. Lee, L. Viciu, L. Li, Y. Wang, M. L. Foo, S. Watauchi, R. A. Pascal, Jr., R. J. Cava, and N. P. Ong, Nature Mater. **5**, 537 (2006).
[5] K. Takada, H. Sakurai, E. Takayama-Muromachi, F. Izumi, R. A. Dilanian, and T. Sasaki, Nature (London) **422**, 53 (2003).
[6] R. E. Schaak, T. Klimczuk, M. L. Foo, and R. J. Cava, Nature (London) **424**, 527 (2003).
[7] P. S. Liu, G. Chen, J. Pei, Y. Cui, D. Q. Lu, N. Zhou, and H. Z. Xian, Physica B **403**, 1808 (2008).
[8] Y. Q. Guo, J. L. Luo, G. T. Liu, H. X. Yang, J. Q. Li, N. L. Wang, and D. Jin, Phys. Rev. B **74**, 155129 (2006).
[9] K. Sugiura, H. Ohta, K. Nomura, M. Hirano, H. Hosono, and K. Koumoto, Appl. Phys. Lett. **88**, 082109 (2006).
[10] K. Yubuta, Y. Hasegawa, Y. Miyazaki, and T. Kajitani, Jpn. J. Appl. Phys., Part 1 **46**, 712 (2007).
[11] M. L. Foo, Y. Wang, S. Watauchi, H. W. Zandbergen, T. He, R. J. Cava, and N. P. Ong, Phys. Rev. Lett. **92**, 247001 (2004).
[12] Q. Huang, M. L. Foo, J. W. Lynn, H. W. Zandbergen, G. Lawes, Y. Wang, B. H. Toby, A. P. Ramirez, N. P. Ong, and R. J. Cava, J. Phys.: Condens. Matter **16**, 5803 (2004).
[13] M. Roger, D. J. P. Morris, D. A. Tennant, M. J. Gutmann, J. P. Goff, J.-U. Hoffmann, R. Feyerherm, E. Dudzik, D. Prabhakaran, A. T. Boothroyd, N. Shannon, B. Lake, and P. P. Deen, Nature (London) **445**, 631 (2007).
[14] H. X. Yang, Y. G. Shi, Y. Q. Guo, X. Liu, R. J. Xiao, J. L. Luo, and J. Q. Li, Mater. Res. Bull. **42**, 94 (2007).
[15] P. Zhang, R. B. Capaz, M. L. Cohen, and S. G. Louie, Phys. Rev. B **71**, 153102 (2005).
[16] H. W. Zandbergen, M. L. Foo, Q. Xu, V. Kumar, and R. J. Cava, Phys. Rev. B **70**, 024101 (2004).
[17] L. Viciu, J. W. G. Bos, H. W. Zandbergen, Q. Huang, M. L. Foo, S. Ishiwata, A. P. Ramirez, M. Lee, and N. P. Ong, Phys. Rev. B **73**, 174104 (2006).
[18] L. D. Yao, Y. Q. Guo, J. L. Luo, W. Zhang, F. Y. Li, C. Q. Jin, and R. C. Yu, Phys. Rev. B **75**, 174118 (2007).
[19] H. X. Yang, Y. G. Shi, X. Liu, R. J. Xiao, H. F. Tian, and J. Q. Li, Phys. Rev. B **73**, 014109 (2006).
[20] K. Sugiura, H. Ohta, Y. Ishida, R. Huang, T. Saito, Y. Ikuhara, K. Nomura, H. Hosono, and K. Koumoto (unpublished).
[21] S. J. Pennycook and D. E. Jesson, Ultramicroscopy **37**, 14 (1991).
[22] J. P. Buban, K. Matsunaga, J. Chen, N. Shibata, W. Y. Ching, T. Yamamoto, and Y. Ikuhara, Science **311**, 212 (2006).
[23] H. Ohta, S. Kim, S. Ohta, K. Koumoto, M. Hirano, and H. Hosono, Cryst. Growth Des. **5**, 25 (2005).
[24] K. Sugiura, H. Ohta, K. Nomura, M. Hirano, H. Hosono, and K. Koumoto, Appl. Phys. Lett. **89**, 032111 (2006).

Downloaded 28 Jul 2009 to 133.6.32.19. Redistribution subject to AIP license or copyright; see http://apl.aip.org/apl/copyright.jsp